

---

# Fuzzy c-Means Clustering for Persistence Diagrams

---

**Thomas O. M. Davies**  
University of Southampton  
t.o.m.davies@soton.ac.uk

**Jack Aspinall**  
University of Oxford  
jack.aspinall@materials.ox.ac.uk

**Bryan Wilder**  
Harvard University  
bwilder@g.harvard.edu

**Long Tran-Thanh**  
University of Southampton  
L.Tran-Thanh@soton.ac.uk

## Abstract

Persistence diagrams, a key tool in the field of Topological Data Analysis, concisely represent the topology of a point cloud. Most current methods to integrate persistence diagrams into machine learning either require prior knowledge of a ground-truth topology or map them into a feature vector, offering a trade-off between information loss and invoking the curse of dimensionality. In this paper we give an algorithm for Fuzzy c-Means (FCM) clustering directly on the space of persistence diagrams, enabling unsupervised learning that automatically captures the topological structure of data, with no prior knowledge or additional processing of persistence diagrams. We prove the same convergence guarantees as traditional FCM clustering: that any convergent subsequence of our algorithm tends to a local minimum or saddle point of the cost function. We end by presenting experiments that demonstrate our algorithm can successfully cluster transformed datasets from materials science where comparable Wasserstein barycentre clustering algorithms fail, whilst also running at least an order of magnitude faster.

## 1 Introduction

Persistence diagrams, a concise representation of the topology of a point cloud, have emerged as a new tool in the field of data analysis [11]. Persistence diagrams have been successfully applied in fields ranging from signal processing to cancer science, but are typically used as exploratory tools with significant input from domain experts [4, 26]. It has proven hard to integrate them into existing machine learning methods, as they are multisets in the extended plane. One current approach adds a topological loss term to the objective function, but this offers only topological regularisation or comparison to some ground-truth persistence diagram [8, 13, 15]. In this case, prior knowledge about the dataset is required, which is clearly not feasible for all problems. Another solution maps persistence diagrams into a feature vector by integrating weighted Gaussians centred at each point over a grid [7, 19]. This embeds the persistence diagram into a finite vector that can be used as an input to most machine learning methods, but requires a trade-off: if the grid is coarse you can lose significant information about the persistence diagram; if the grid is fine then you embed into a high dimensional space and come up against the curse of dimensionality.

Against this background, we give an algorithm to perform Fuzzy c-Means (FCM) clustering *directly* on collections of persistence diagrams of data points, tackling an important unsupervised learning problem and enabling learning from persistence diagrams without mapping into a different space. By clustering persistence diagrams we group together datasets with the same shape, revealing commonalities between data that may not be immediately obvious. Unlike existing algorithms for hard clustering [24], fuzzy clustering gives each diagram a fractional membership value for every cluster. This lets datasets with the same topology, but dissimilar geometry, have partial memberships

to clusters that represent distinct features in a manner impossible with discrete labels; enabling our algorithm to capture more nuanced information. Continuous membership values have also been shown to be more robust than discrete labels [20]. However, the extension to fuzzy clustering comes with theoretical challenges not present in hard clustering, as the weighted cost function makes the convergence analysis non-trivial.

## 1.1 Our contributions

1. Our main contribution is an algorithm for Fuzzy c-Means clustering of persistence diagrams. Given a collection of persistence diagrams  $\mathbb{D}_1, \dots, \mathbb{D}_n$ , we alternatively calculate cluster centres  $\mathbb{M}_1, \dots, \mathbb{M}_c$  and membership values  $r_{jk} \in [0, 1]$  which denote the degree to which diagram  $\mathbb{D}_j$  is associated with cluster  $\mathbb{M}_k$ . Note that the cluster centres are themselves in the space of persistence diagrams. Theorem 2 states that every convergent subsequence of these alternative update steps tends to a local minimum or saddle point of the cost function. This is the same convergence guarantee provided by traditional FCM clustering [3]. We use Zangwill’s Convergence Theorem to prove this result, which requires proving that the sequence is contained within a compact set, that the cost function is a descent function, and that the algorithm is closed on the complement of the solution set. We prove these requirements in Appendix A.

2. Updating the cluster centres requires computing an extension of centroids to metric spaces called the weighted Fréchet mean. We provide the first algorithm that computes the weighted Fréchet mean of persistence diagrams. In Theorem 3, proven in Appendix B, we show that this algorithm converges to a local minimum by extending work in [29] that defines a tangent cone on the space of persistence diagrams.

3. We implement our algorithm in Python, available at <https://github.com/tomogwen/fpdccluster>. It works with persistence diagrams from the open-source library Dionysus,<sup>1</sup> so is available for easy integration into current workflows. In the experiments section, we give timing results showing that our algorithm is at least an order of magnitude faster than comparable Wasserstein barycentre clustering algorithms. We test our algorithm on two datasets from materials science: cubic structures and carbon allotropes. Cubic structures are important because they are ubiquitous: the most common lattice structures are face-centred cubic structures and body-centred cubic structures [28]. Carbon allotropes such as graphene and diamond are widely anticipated to revolutionise electronics and optoelectronics [30, 32] and have been central to some of the most high-profile materials research. A key property for machine learning in materials science has been identified as “invariance to the basis symmetries of physics... rotation, reflection, translation” [18]. Removing the need for a standardised coordinate system allows machine learning methods to be applied to a broader range of existing coordinate datasets. We show that our algorithm can successfully cluster these datasets regardless of rotation, reflection, and translation of the underlying data, where comparable clustering algorithms fail.

To sum up, our method provides the following advantages compared to existing solutions: By mapping a dataset to a planar summary of its topology, persistence diagrams intrinsically perform dimensionality reduction whilst summarising the important information about the topology. In testing we find this offers a speed increase of at least an order of magnitude over comparable Wasserstein barycentre clustering algorithms. Persistence diagrams also offer invariance to rotations, translations, and reflections of the underlying dataset, giving our algorithm the same property.

## 1.2 Related work

We build on recent work in Topological Data Analysis that proposes hard clustering for persistence diagrams [24]. This work uses an algorithm to compute (unweighted) Fréchet means [29] that we extend to the weighted case. Our method also builds on top of the FCM clustering algorithm, originally developed by Bezdek [2]. We use modified versions of his update procedures, as well as generalising his proof to persistence diagrams. The most similar unsupervised learning technique to our algorithm is Wasserstein Barycentre Clustering (WBC). It clusters datasets of point clouds by the Wasserstein distance between the point clouds, rather than the Wasserstein distance between their persistence diagrams. We compare our algorithm experimentally to WBC using ADMM [33], Bregman ADMM [34], Subgradient Descent [9], Iterative Bregman Projection [1], and full linear

---

<sup>1</sup><https://github.com/mrzv/dionysus>

programming [22]. Each of these algorithms computes or approximates the Wasserstein barycentre in different ways. Theoretically, fuzzy discrete distribution clustering [10] offers similarities to our algorithm. In comparison, our work clusters persistence diagrams rather than discrete distributions and uses the Fréchet mean to update centroids. Persistence diagrams have also been used to determine the correct number of clusters for clustering on Riemmanian manifolds [5, 27].

Other work has developed different techniques to integrate persistence diagrams into machine learning. The form of persistence diagrams presents challenges: they are multisets in the extended plane that can vary in cardinality based on the topology of the underlying data. To overcome this, some solutions add a topological loss to an objective function. However, this only offers topological regularisation or comparison to some ground-truth persistence diagram [8, 13, 15]. Both require prior knowledge of the correct topology and so are not feasible for general applications. Another solution maps persistence diagrams into a finite vector by placing weighted Gaussians at each point in the persistence diagram and integrating over a grid [7]. This requires a trade-off: if the grid is too coarse you lose information, as points could be anywhere within a section of the grid. If the grid is too fine, then you embed the persistence diagram into a very high dimensional vector, and you come up against the curse of dimensionality. Importantly for any gradient descent approaches, a thorough analysis of the differentiability of persistence diagrams has also been completed [21].

## 2 Topological preliminaries

Topological Data Analysis emerged from the study of algebraic topology, providing a toolkit to fully describe the topology of a dataset. We offer a quick summary below; for more comprehensive details see [11]. A set of points in  $\mathbb{R}^d$  are indicative of the shape of the distribution they are sampled from. By placing a ball of radius  $\epsilon > 0$  around each point and connecting points where balls intersect, we can create an approximation of the distribution, called the Čech complex. Specifically, we add the convex hull of  $k$  points to the  $\epsilon$ -Čech complex when the corresponding  $k$  balls intersect in a single point. As we increase  $\epsilon$ , more balls intersect, changing the granularity of our approximation of the distribution. An example of this is shown in Figure 1(a). In our implementation we use a very similar, but more computationally efficient, construction called the Rips complex. This is constructed by adding the convex hull of any collection of points that are pairwise at most  $\epsilon$  apart to the  $\epsilon$ -Rips complex. The collection of complexes for all  $\epsilon$  is called a filtration.

For each  $\epsilon$ , we compute the  $p$ -homology group. This tells us the topology of the  $\epsilon$ -Rips complex: the 0-homology counts the number of connected components, the 1-homology counts the number of holes, the 2-homology counts the number of voids, and so on [12]. The  $p$ -persistent homology ( $p$ -PH) group is then created by summing the  $p$ -homology groups over all  $\epsilon$ . This results in a  $p$ -PH group that summarises information about the topology of the dataset at all granularities. If a topological feature, such as a connected component or hole, persists throughout a large range of granularities, then it's more likely to be a feature of the distribution. If it only persists for a short amount of time, then it's more likely to be noise. We can stably map a  $p$ -PH group into a multiset in the extended plane called a persistence diagram [6]. Each topological feature has a birth and death: a feature is born when it enters the complex, and dies when the complex grows enough to destroy it. For example, in Figure 1(a), a feature is born at  $\epsilon = 8$  when three lines form a hole. This feature dies at  $\epsilon = 9$  when the hole is filled in. This is shown in the persistence diagram in Figure 1(b) as a point at  $(8, 9)$  in 1-PH. By computing the birth/death points for each topological feature in the filtration [36], we get a complete picture of the topology of the point cloud at all granularities.

## 3 Algorithmic design

### 3.1 Clustering persistence diagrams

We use the 2-Wasserstein  $L_2$  distance as a metric on the space of persistence diagrams as it is stable on persistence diagrams of finite point clouds [6]. The Wasserstein distance is an optimal transport metric that has found applications across machine learning. In the Euclidean case, it quantifies the smallest distance between optimally matched points. Most pertinent to us is its application in Wasserstein barycentre clustering, a technique to cluster discrete distributions that is comparable to

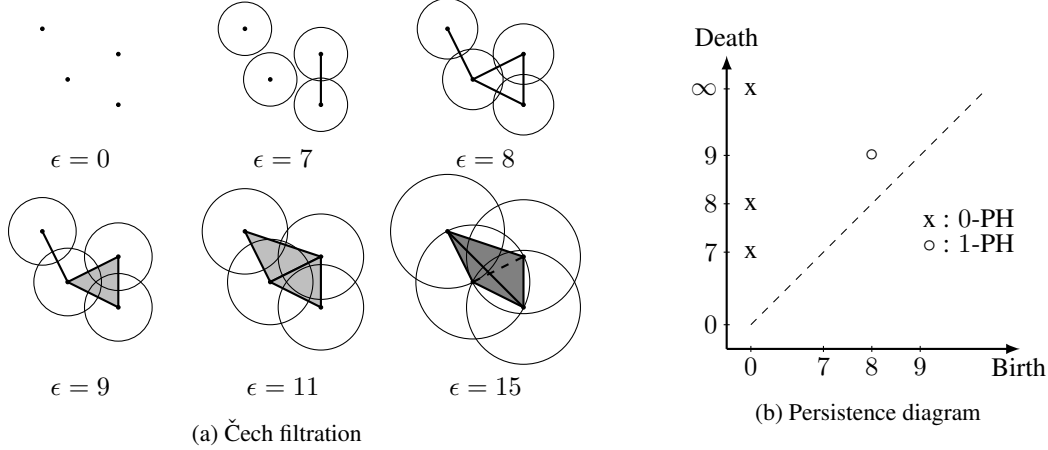


Figure 1: Čech filtration with its persistence diagram

persistence diagram clustering. Given diagrams  $\mathbb{D}_1, \mathbb{D}_2$ , the distance is

$$W_2(\mathbb{D}_1, \mathbb{D}_2) = \left( \inf_{\gamma: \mathbb{D}_1 \rightarrow \mathbb{D}_2} \sum_{x \in \mathbb{D}_1} \|x - \gamma(x)\|_2^2 \right)^{1/2},$$

where the infimum is taken over all bijections  $\gamma: \mathbb{D}_1 \rightarrow \mathbb{D}_2$ . In order for the Wasserstein distance to be well defined between persistence diagrams with different numbers of points, we add copies of the diagonal  $\Delta$  to each diagram so that every diagram has the same total number of off-diagonal points, and copies of the diagonal. If an off-diagonal point is matched to the diagonal the transportation cost is simply the shortest distance to the diagonal. In fact, the closer a point is to the diagonal, the more likely it is to be noise, so this ensures our distance is not overly affected by noise.

We work in the space  $\mathcal{D}_{L^2} = \{\mathbb{D} : W_2(\mathbb{D}, \Delta) < \infty\}$ ,<sup>2</sup> as this leads to a geodesic space with known structure [29]. Given a collection of persistence diagrams  $\{\mathbb{D}_j\}_{j=1}^n \subset \mathcal{D}_{L^2}$  and a fixed number of clusters  $c$ , we wish to find cluster centres  $\{\mathbb{M}_k\}_{k=1}^c \subset \mathcal{D}_{L^2}$ , along with membership values  $r_{jk} \in [0, 1]$  that denote the extent to which  $\mathbb{D}_j$  is associated with cluster  $\mathbb{M}_k$ . We follow probabilistic fuzzy clustering, so that  $\sum_k r_{jk} = 1$  for each  $j$ .

We extend the hard persistence diagram clustering algorithm in [24] to reflect the Fuzzy c-Means algorithm originally proposed by Bezdek [2]. Our  $r_{jk}$  is the same as traditional FCM clustering, adapted with the Wasserstein distance. That is,

$$r_{jk} = \left( \sum_{l=1}^c \frac{W_2(\mathbb{M}_k, \mathbb{D}_j)}{W_2(\mathbb{M}_l, \mathbb{D}_j)} \right)^{-1}. \quad (1)$$

In order to update the cluster centres, we need a generalisation of centroids to metric spaces called the Fréchet mean.

**Definition 1.** Given a complete metric space  $(X, d)$ , a set of points  $x_1, \dots, x_n \in X$ , and a set of associated weights  $w_1, \dots, w_n \in \mathbb{R}$ , the weighted Fréchet variance, or Fréchet function, of a point  $p \in X$  is  $\sum_{i=1}^n w_i d(p, x_i)^2$ . The Fréchet mean is a point  $p$  that is a global minimum of the Fréchet function.

<sup>2</sup>To ensure that our persistence diagrams are all in this space, we map points at infinity to a hyperparameter  $T$  that is much larger than other death values in the diagram. As we're using the Rips complex, there will only ever be one point at infinity (which will be in 0-PH). This hyperparameter ensures that the one point at infinity will always be matched to the corresponding point at infinity when computing the Wasserstein distance between diagrams.

To update  $\mathbb{M}_k$ , we compute the weighted Fréchet mean of the persistence diagrams  $\{\mathbb{D}_j\}_{j=1}^n$  with the weights  $\{r_{jk}^2\}_{j=1}^n$ . Specifically,

$$\mathbb{M}_k \leftarrow \arg \min_{\hat{\mathbb{D}}} \sum_{j=1}^n r_{jk}^2 W_2(\hat{\mathbb{D}}, \mathbb{D}_j)^2, \text{ for } k = 1, \dots, c. \quad (2)$$

As the weighted Fréchet mean extends weighted centroids to  $\mathcal{D}_{L^2}$ , this gives our fuzzy cluster centres. The computation of the weighted Fréchet mean is covered in Section 3.2. By alternatively updating (1) and (2) we get a sequence of iterates. Theorem 2, proven in Appendix A, provides the same convergence guarantees as traditional FCM clustering.

**Theorem 2.** *Every convergent subsequence of the sequence of iterates obtained by alternatively updating membership values and cluster centres with (1) and (2) tends to a local minimum or saddle point of the cost function  $J(R, \mathbb{M}) = \sum_{j=1}^n \sum_{k=1}^c r_{jk}^2 W_2(\mathbb{M}_k, \mathbb{D}_j)^2$ .*

Observe that we only guarantee the convergence of subsequences of iterates. This is the same as traditional FCM clustering, so we follow the same approach to a stopping condition and run our algorithm for a fixed number of iterations. The entire algorithm is displayed in Algorithm 1.

---

**Algorithm 1** FPDCluster

---

**Input** Diagrams  $\mathbb{D} = \{\mathbb{D}_j\}_{j=1}^n$ , number of clusters  $c$ , maximum iterations MAXITER

**Output** Cluster centres  $\mathbb{M} = \{\mathbb{M}_k\}_{k=1}^c$ , membership values  $R = \{r_{jk}\}$

---

```

1:  $\mathbb{D} = \text{ADDDIAGONALS}(\mathbb{D})$ 
2:  $\mathbb{M} = \text{INITCENTRES}(\mathbb{D})$ 
3: for count in 1..MAXITER do
4:   for  $j$  in 1.. $n$  do
5:     for  $k$  in 1.. $c$  do
6:        $r_{jk} \leftarrow \left( \sum_{l=1}^c \frac{W_2(\mathbb{M}_k, \mathbb{D}_j)}{W_2(\mathbb{M}_l, \mathbb{D}_j)} \right)^{-1}$ 
7:     end for
8:   end for
9:   for  $k$  in 1.. $c$  do
10:     $\mathbb{M}_k \leftarrow \text{WFRECHETMEAN}(\mathbb{D}, R_k)$ 
11:   end for
12: end for
13: return  $\mathbb{M}, R$ 

```

---

### 3.2 Computing the weighted Fréchet mean

In Algorithm 1 we added copies of the diagonal to ensure that each diagram has the same cardinality; denote this cardinality as  $m$ . To compute the weighted Fréchet mean, we need to find  $\mathbb{M}_k = \{y^{(i)}\}_{i=1}^m$  that minimises the Fréchet function in (2). Implicit to the Wasserstein distance is a bijection  $\gamma_j : y^{(i)} \mapsto x_j^{(i)}$  for each  $j$ . Supposing we know these bijections, we can rearrange the Fréchet function into the form  $F(\mathbb{M}_k) = \sum_{j=1}^n r_{jk}^2 W_2(\mathbb{M}_k, \mathbb{D}_j)^2 = \sum_{i=1}^m \sum_{j=1}^n r_{jk}^2 \|y^{(i)} - x_j^{(i)}\|^2$ .

In this form, the summand is minimised for  $y^{(i)}$  by the weighted Euclidean centroid of the points  $\{x_j^{(i)}\}_{j=1}^n$ . Therefore to compute the weighted Fréchet mean, we need to find the correct bijections. To this end, we modify the algorithm for the computation of the unweighted case given in [29].

We start by using the Hungarian algorithm to find an optimal matching between  $\mathbb{M}_k$  and each  $\mathbb{D}_j$ . Given a  $\mathbb{D}_j$ , for each point  $y^{(i)} \in \mathbb{M}_k$ , the Hungarian algorithm will assign an optimally matched point  $x_j^{(i)} \in \mathbb{D}_j$ . Specifically, we find matched points

$$\left[ x_j^{(i)} \right]_{i=1}^m \leftarrow \text{Hungarian}(\mathbb{M}_k, \mathbb{D}_j), \text{ for each } j = 1, \dots, n. \quad (3)$$

Now, for each  $y^{(i)} \in \mathbb{M}_k$  we need to find the weighted average of the matched points  $\left[ x_j^{(i)} \right]_{j=1}^n$ . However, some of these points could be copies of the diagonal, so we need to consider three distinct cases: that each matched point is off-diagonal, that each one is a copy of the diagonal, or that the points are a mixture of both. We start by partitioning the diagram indices for each  $i = 1, \dots, n$  into the indices of the off-diagonal points  $\mathcal{J}_{\text{OD}}^{(i)} = \{j : x_j^{(i)} \neq \Delta\}$  and the indices of the diagonal

points  $\mathcal{J}_D^{(i)} = \{j : x_j^{(i)} = \Delta\}$ . Now, if  $\mathcal{J}_{OD} = \emptyset$  then  $y^{(i)}$  is a copy of the diagonal. If not, let  $w = \left(\sum_{j \in \mathcal{J}_{OD}^{(i)}} r_{jk}^2\right)^{-1} \sum_{j \in \mathcal{J}_{OD}^{(i)}} r_{jk}^2 x_j^{(i)}$  be the weighted mean of the off-diagonal points. If  $\mathcal{J}_D^{(i)} = \emptyset$ , then  $y^{(i)} = w$ . Otherwise, let  $w_\Delta$  be the point on the diagonal closest to  $w$ . Then our update is

$$y^{(i)} \leftarrow \frac{\sum_{j \in \mathcal{J}_{OD}^{(i)}} r_{jk}^2 x_j^{(i)} + \sum_{j \in \mathcal{J}_D^{(i)}} r_{jk}^2 w_\Delta}{\sum_{j=1}^n r_{jk}^2}, \text{ for } i = 1, \dots, m. \quad (4)$$

We summarise this process in Algorithm 2. Theorem 3, proving that Algorithm 2 terminates at a local minimum of the Fréchet function, is proven in Appendix B.

**Theorem 3.** *Given diagrams  $\mathbb{D}_j$ , membership values  $r_{jk}$ , and the Fréchet function  $F(\hat{\mathbb{D}}) = \sum_{j=1}^n r_{j,k}^2 W_2(\hat{\mathbb{D}}, \mathbb{D}_j)^2$ , then  $\mathbb{M}_k = \{y^{(i)}\}_{i=1}^m$  is a local minimum of  $F$  if and only if there is a unique optimal pairing from  $\mathbb{M}_k$  to each of the  $\mathbb{D}_j$  and each  $y^{(i)}$  is updated via (4).*

---

#### Algorithm 2 WFréchetMean

---

**Input** Diagrams  $\mathbb{D} = \{\mathbb{D}_j\}_{j=1}^n$ , Weights  $R_k = \{r_{jk}\}_{j=1}^n$  (fixed  $k$ )  
**Output** Weighted Fréchet mean  $\mathbb{M}_k = \{y^{(i)}\}_{i=1}^m$

```

1:  $m \leftarrow \max_{1 \leq j \leq n} |\mathbb{D}_j|$ 
2: for  $j$  in  $1..n$  do
3:    $\left[x_j^{(i)}\right]_{i=1}^m \leftarrow \text{HUNGARIAN}(\mathbb{M}_k, \mathbb{D}_j)$ 
4: end for
5: while  $\left\{\left[x_j^{(i)}\right]_{i=1}^m\right\}_{j=1}^n \neq \left\{\left[\hat{x}_j^{(i)}\right]_{i=1}^m\right\}_{j=1}^n$ 
6:   for  $i$  in  $1..m$  do
7:      $\mathcal{J}_{OD}^{(i)} = \{j : x_j^{(i)} \neq \Delta\}$ 
8:      $\mathcal{J}_D^{(i)} = \{j : x_j^{(i)} = \Delta\}$ 
9:     if  $\mathcal{J}_{OD}^{(i)} = \emptyset$  then
10:       $y^{(i)} \leftarrow \Delta$ 
11:     else
12:       $w = \left(\sum_{j \in \mathcal{J}_{OD}^{(i)}} r_{jk}^2\right)^{-1} \sum_{j \in \mathcal{J}_{OD}^{(i)}} r_{jk}^2 x_j^{(i)}$ 
13:      if  $\mathcal{J}_D^{(i)} = \emptyset$  then
14:         $y^{(i)} \leftarrow w$ 
15:      else
16:         $y^{(i)} \leftarrow \frac{\sum_{j \in \mathcal{J}_{OD}^{(i)}} r_{jk}^2 x_j^{(i)} + \sum_{j \in \mathcal{J}_D^{(i)}} r_{jk}^2 w_\Delta}{\sum_{j=1}^n r_{jk}^2}$ 
17:     end if
18:   end if
19: end for
20:  $\left\{\left[\hat{x}_j^{(i)}\right]_{i=1}^m\right\}_{j=1}^n \leftarrow \left\{\left[x_j^{(i)}\right]_{i=1}^m\right\}_{j=1}^n$ 
21: for  $j$  in  $1..n$  do
22:    $\left[x_j^{(i)}\right]_{i=1}^m \leftarrow \text{HUNGARIAN}(\mathbb{M}_k, \mathbb{D}_j)$ 
23: end for
24: end while
25: return  $\{y^{(i)}\}_{i=1}^m$ 

```

---

## 4 Experiments

### 4.1 Synthetic data

We start by demonstrating our algorithm on a simple synthetic dataset designed to highlight its ability to cluster based on the topology of the underlying datasets. We produce three datasets of noise, three datasets of a ring, and three datasets of figure-of-eights, all shown in Figure 2(a). In Figure 2(b) we show the corresponding 1-PH persistence diagrams. Note that the persistence diagrams have either zero, one, or two significant off-diagonal points, corresponding to zero, one, or two rings in the datasets. We then use our algorithm to cluster the nine persistence diagrams into three clusters. Having only been given the list of diagrams, the number of clusters, and the maximum number of iterations, our algorithm successfully clusters the diagrams. Figure 2(c) shows that the cluster centres

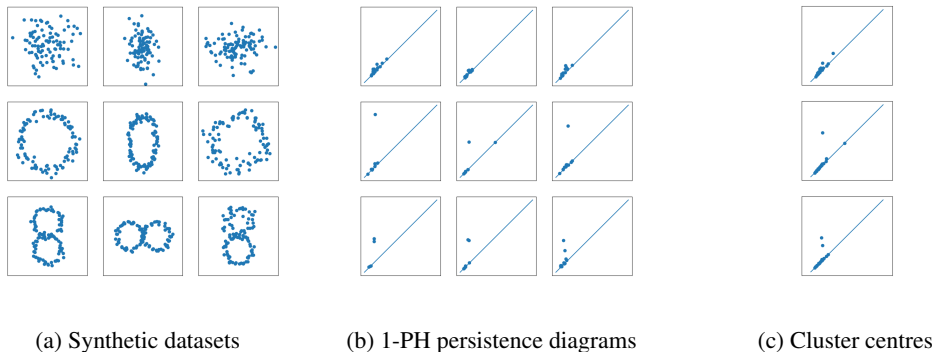


Figure 2: Our algorithm successfully clustered the persistence diagrams, finding cluster centres that represent the topology of the datasets

Table 1: Seconds per clustering iteration

Points	100	200	300	400	500	600	700	800	900	1000
<b>FPDCluster</b>	<b>0.01552</b>	<b>0.1975</b>	<b>0.9358</b>	<b>2.229</b>	<b>5.694</b>	<b>12.29</b>	<b>19.27</b>	<b>34.50</b>	<b>53.20</b>	<b>77.81</b>
ADMM	5.622	34.86	161.3	617.6	-	-	-	-	-	-
BADMM	0.2020	2.188	26.38	112.6	-	-	-	-	-	-
SubGD	0.4217	2.273	22.17	103.4	-	-	-	-	-	-
IterBP	0.3825	2.226	21.57	108.9	-	-	-	-	-	-
LP	0.3922	2.031	22.32	117.3	-	-	-	-	-	-

have zero, one, or two off-diagonal points: our algorithm has found cluster centres that reflect the topological features of the datasets.

We also use synthetic data to empirically compare the running time of our algorithm to other dataset clustering algorithms available. Computing the Wasserstein distance has super-cubic time complexity [23], so is a significant bottleneck both for our algorithm and comparable Wasserstein barycentre clustering algorithms [1, 9, 22, 33, 34]. Persistence diagrams generally reduce both the dimensionality and number of points in a dataset,<sup>3</sup> so we in turn reduce the computational bottleneck. To demonstrate this, we evaluated the average time per iteration of our persistence diagram clustering algorithm, as well as the average iteration time for comparable Wasserstein barycentre clustering algorithms. We included the time taken to compute the persistence diagrams from the datasets when timing our clustering algorithm. We give the results in Table 1, leaving an entry blank where it became unpractical to run a test (e.g. it takes too long to return a solution and the algorithm becomes unresponsive). We show at least an order of magnitude improvement in performance over comparable Wasserstein barycentre clustering algorithms.<sup>4</sup>

## 4.2 Lattice structures

The large majority of solids are comprised of lattices: regularly repeating unit cells of atoms. This lattice structure directly determines the properties of a material [16] and it has been predicted that machine learning will reveal presently unknown links between structure and property by identifying new trends across materials [25, 31]. We apply our algorithm to two examples of lattice structures from materials science: cubic structures and carbon allotropes. Cubic structures are important because they are ubiquitous. The most common lattice structures, particularly amongst pure metals, are face-centred cubic (FCC) structures and body-centred cubic (BCC) structures [28], shown in Figures 3(a) and 3(b). Carbon allotropes, such as graphene and diamond, are widely anticipated to

<sup>3</sup>Persistence diagrams are always planar, so if the data is in  $\mathbb{R}^d$ ,  $d > 2$ , then there is a dimensionality reduction. For  $p > 0$ , the persistence diagram of  $p$ -PH always has less points than the dataset when computed with the Rips complex.

<sup>4</sup>Further details of the experimental setup is available in Appendix C.

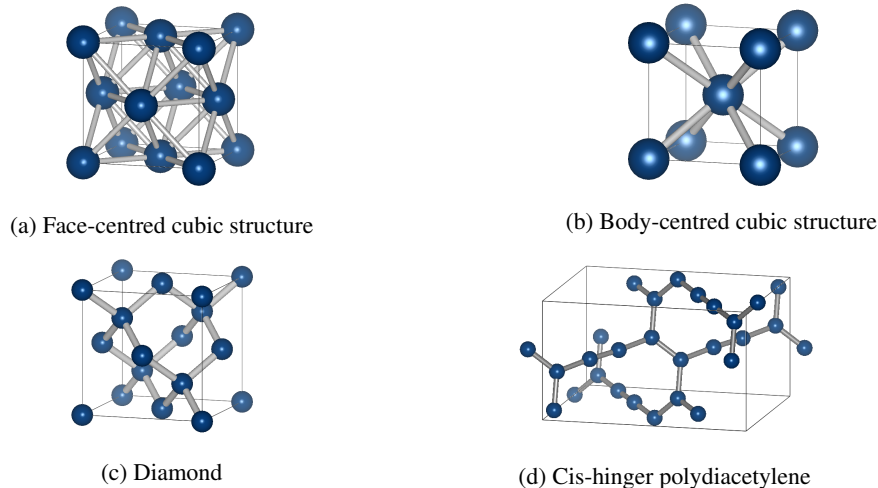


Figure 3: Cubic structures (top) and carbon allotropes (bottom)

revolutionise electronics and optoelectronics [30, 32]. We focus on the carbon allotropes diamond and cis-hinged polydiacetylene, shown in Figures 3(c) and 3(d).

A key property for machine learning in materials science has been identified as “invariance to the basis symmetries of physics... rotation, reflection, translation” [18]. Removing the need for a standardised coordinate system allows machine learning methods to be applied to a broader range of existing coordinate datasets generated by experimental methods such as x-ray diffraction and scanning electron microscope imaging, and computational methods such as density functional theory. We use atomic positions for the unit-cells of iron mp-150 and iron mp-13 from the Materials Project [17], representing BCC and FCC structures respectively, for our first experiment. For our second experiment we use diamond and cis-hinged polydiacetylene unit-cell atomic positions from the Samara Carbon Allotrope Database [14]. We simulate distinct collections of lattices by transforming the atomic coordinates, with no information about bonds given to the algorithms.

Our persistence diagram clustering is able to successfully cluster together collections of atomic coordinates derived from the same base unit-cell regardless of the transformations applied to the coordinate system, fulfilling the key property identified above (we consider a clustering successful when all datasets from the same lattice structure have their highest membership values for the same cluster). In comparison, we run Wasserstein barycentre clustering on the same datasets using several state-of-the-art algorithms for barycentre computation and approximation. Each can only successfully cluster the cubic structures after reflection, and none of them successfully cluster the carbon allotropes after any transformations. We show these results in Table 2 and provide expanded results in Appendix C.2.

Table 2: Clustering results after transformation

	Cubic Structures				Carbon Allotropes			
	None	Rotate	Reflect	Translate	None	Rotate	Reflect	Translate
<b>FPDCluster</b>	✓	✓	✓	✓	✓	✓	✓	✓
ADMM	✓	✗	✓	✗	✓	✗	✗	✗
BADMM	✓	✗	✓	✗	✓	✗	✗	✗
SubGD	✓	✗	✓	✗	✓	✗	✗	✗
IterBP	✓	✗	✓	✗	✓	✗	✗	✗
LP	✓	✗	✓	✗	✓	✗	✗	✗



## 5 Conclusion

We have developed FCM clustering on the space of persistence diagrams, adding an important class of unsupervised learning to Topological Data Analysis’ toolkit. Our algorithm successfully clusters transformed lattice structures where comparable Wasserstein barycentre clustering techniques fail, whilst offering an improvement in running time of at least an order of magnitude. In the future, we envisage our algorithm being used as a key step in automated materials discovery, clustering large datasets from across materials science to discover currently unknown links between lattice structure and material properties. We plan to extend our algorithm to topologically cluster graphs as our future work. This would involve learning a process to interpret graphs as filtrations.

## Broader impact

Our paper focuses on a theoretical contribution, offering a new topological clustering technique for datasets. We analyse an application of our algorithm to materials science, demonstrating that it can cluster materials with the same lattice structure together regardless of transformations to the underlying coordinates. This has potential applications in automated materials discovery, an area of materials science that seeks to find new materials with novel properties. Currently targeted materials have applications varying from solar cells and battery technology, to future replacements for silicon electronics. Whilst any scientific innovation can have positive or negative impacts, we hope that any future application of our work to materials discovery contributes a net good to the world.

## References

- [1] J.-D. BENAMOU, G. CARLIER, M. CUTURI, L. NENNA, AND G. PEYRÉ, *Iterative bregman projections for regularized transportation problems*, SIAM Journal on Scientific Computing, (2015).
- [2] J. C. BEZDEK, *A convergence theorem for the fuzzy isodata clustering algorithms*, IEEE Transactions on Pattern Analysis and Machine Intelligence, PAMI-2 (1980), pp. 1–8.
- [3] J. C. BEZDEK, R. J. HATHAWAY, M. J. SABIN, AND W. T. TUCKER, *Convergence theory for fuzzy c-means: Counterexamples and repairs*, IEEE Transactions on Systems, Man, and Cybernetics, 17 (1987), pp. 873–877.
- [4] H. BOCHE, M. GUILLEMARD, G. KUTYNIOK, AND F. PHILIPP, *Signal analysis with frame theory and persistent homology*, 01 2013.
- [5] F. CHAZAL, L. GUIBAS, S. OUDOT, AND P. SKRABA, *Persistence-based clustering in riemannian manifolds*, Journal of the ACM, 60 (2011).
- [6] F. CHAZAL, V. SILVA, M. GLISSE, AND S. OUDOT, *The Structure and Stability of Persistence Modules*, 07 2012.
- [7] S. CHEPUSHTANOVA, T. EMERSON, E. HANSON, M. KIRBY, F. MOTTA, R. NEVILLE, C. PETERSON, P. SHIPMAN, AND L. ZIEGELMEIER, *Persistence images: An alternative persistent homology representation*, (2015).
- [8] J. CLOUGH, I. OKSUZ, N. BYRNE, V. ZIMMER, J. SCHNABEL, AND A. KING, *A topological loss function for deep-learning based image segmentation using persistent homology*, 10 2019.
- [9] M. CUTURI AND A. DOUCET, *Fast computation of wasserstein barycenters*, in Proceedings of the 31st International Conference on Machine Learning, E. P. Xing and T. Jebara, eds., vol. 32 of Proceedings of Machine Learning Research, Beijing, China, 22–24 Jun 2014, PMLR, pp. 685–693.
- [10] F. D. A. T. DE CARVALHO, A. IRPINO, AND R. VERDE, *Fuzzy clustering of distribution-valued data using an adaptive l2 wasserstein distance*, in 2015 IEEE International Conference on Fuzzy Systems (FUZZ-IEEE), 2015, pp. 1–8.
- [11] H. EDELSBRUNNER AND J. HARER, *Computational Topology - an Introduction.*, American Mathematical Society, 2010.

- [12] H. EDELSBRUNNER, D. LETSCHER, AND A. ZOMORODIAN, *Topological persistence and simplification*, vol. 28, 02 2000, pp. 454 – 463.
- [13] R. B. GABRIELSSON, B. J. NELSON, A. DWARAKNATH, P. SKRABA, L. J. GUIBAS, AND G. E. CARLSSON, *A topology layer for machine learning*, CoRR, abs/1905.12200 (2019).
- [14] R. HOFFMANN, A. KABANOV, A. GOLOV, AND D. PROSERPIO, *Homo citans and carbon allotropes: For an ethics of citation*, Angewandte Chemie International Edition, 55 (2016).
- [15] X. HU, F. LI, D. SAMARAS, AND C. CHEN, *Topology-preserving deep image segmentation*, in *Advances in Neural Information Processing Systems 32*, Curran Associates, Inc., 2019, pp. 5657–5668.
- [16] D. HULL AND D. BACON, *Introduction to Dislocations (Fifth Edition)*, Butterworth-Heinemann, Oxford, fifth edition ed., 2011.
- [17] A. JAIN, S. P. ONG, G. HAUTIER, W. CHEN, W. D. RICHARDS, S. DACEK, S. CHOLIA, D. GUNTER, D. SKINNER, G. CEDER, AND K. A. PERSSON, *The Materials Project: A materials genome approach to accelerating materials innovation*, APL Materials, 1 (2013), p. 011002.
- [18] S. B. JONATHAN SCHMIDT, MÁRIO R. G. MARQUES AND M. A. L. MARQUES, *Recent advances and applications of machine learning in solid-state materials science*, npj Computational Materials, 5 (2019), p. 83.
- [19] M. KIMURA, I. OBAYASHI, Y. TAKEICHI, R. MURAO, AND Y. HIRAOKA, *Non-empirical identification of trigger sites in heterogeneous processes using persistent homology*, Scientific Reports, 8 (2018).
- [20] F. KLAWONN, *Fuzzy clustering: Insights and a new approach*, Mathware & soft computing, ISSN 1134-5632, Vol. 11, N<sup>o</sup>. 3, 2004, pags. 125-142, 11 (2004).
- [21] J. LEYGONIE, S. OUDOT, AND U. TILLMANN, *A framework for differential calculus on persistence barcodes*, 10 2019.
- [22] J. LI AND J. Z. WANG, *Real-time computerized annotation of pictures*, IEEE Transactions on Pattern Analysis and Machine Intelligence, 30 (2008), pp. 985–1002.
- [23] H. LING AND K. OKADA, *An efficient earth mover’s distance algorithm for robust histogram comparison*, IEEE Transactions on Pattern Analysis and Machine Intelligence, 29 (2007), pp. 840–853.
- [24] V. MAROULAS, J. MIKE, AND A. MARCHESI, *K-means clustering on the space of persistence diagrams*, in SPIE, 08 2017, p. 29.
- [25] B. MEREDIG, *Five high-impact research areas in machine learning for materials science*, Chemistry of Materials, 31 (2019), pp. 9579–9581.
- [26] M. NICOLAU, A. J. LEVINE, AND G. CARLSSON, *Topology based data analysis identifies a subgroup of breast cancers with a unique mutational profile and excellent survival*, Proceedings of the National Academy of Sciences, 108 (2011), pp. 7265–7270.
- [27] J. A. PIKE, A. O. KHAN, C. PALLINI, S. G. THOMAS, M. MUND, J. RIES, N. S. POULTER, AND I. B. STYLES, *Topological data analysis quantifies biological nano-structure from single molecule localization microscopy*, Bioinformatics, 36 (2019), pp. 1614–1621.
- [28] A. PUTNIS, *An Introduction to Mineral Sciences*, Cambridge University Press, 1992.
- [29] K. TURNER, Y. MILEYKO, S. MUKHERJEE, AND J. HARER, *Fréchet means for distributions of persistence diagrams*, Discrete & Computational Geometry, 52 (2012), pp. 44–70.
- [30] Z. WANG, F. DONG, B. SHEN, R. ZHANG, Y. ZHENG, L. CHEN, S. WANG, C. WANG, K. HO, Y.-J. FAN, B.-Y. JIN, AND W.-S. SU, *Electronic and optical properties of novel carbon allotropes*, Carbon, 101 (2016), pp. 77–85.

- [31] J. WEI, X. CHU, X. SUN, K. XU, H. DENG, J. CHEN, Z. WEI, AND M. LEI, *Machine learning in materials science*, InfoMat, 1 (2019), pp. 338–358.
- [32] Y. WU, D. FARMER, F. XIA, AND P. AVOURIS, *Graphene electronics: Materials, devices, and circuits*, Proceedings of the IEEE, 101 (2013), pp. 1620–1637.
- [33] J. YE AND J. LI, *Scaling up discrete distribution clustering using admm*, in 2014 IEEE International Conference on Image Processing (ICIP), 2014, pp. 5267–5271.
- [34] J. YE, P. WU, J. WANG, AND J. LI, *Fast discrete distribution clustering using wasserstein barycenter with sparse support*, IEEE Transactions on Signal Processing, PP (2017), pp. 1–1.
- [35] W. ZANGWILL, *Nonlinear programming: a unified approach*, Prentice-Hall international series in management, Prentice-Hall, 1969.
- [36] A. ZOMORODIAN AND G. CARLSSON, *Computing Persistent Homology*, Discrete & Computational Geometry, 33 (2005), pp. 249–274.

## A Convergence of the FCM clustering algorithm

We first need to consider our separate updates as a single update procedure. Let  $F : \mathbb{M} \mapsto R$  be defined by (1) and  $G : R \mapsto \mathbb{M}$  be defined by (2), and for  $R = \{r_{jk}\}$  and  $\mathbb{M} = \{\mathbb{M}_k\}$  consider the sequence

$$\left\{ T^{(l)}(R, \mathbb{M}) : l = 0, 1, \dots \right\}, \text{ where } T(R, M) = (F \circ G(R), G(R)).$$

We wish to show convergence of the iterates of  $T$  to a local minimum or saddle point of the cost function

$$J(R, \mathbb{M}) = \sum_{j=1}^n \sum_{k=1}^c r_{jk}^2 W_2(\mathbb{M}_k, \mathbb{D}_j)^2.$$

The two stage update process of  $T$  is too complicated to use standard fixed point theorems, so as in [2] we shall use the following result, which is proven in [35].

**Theorem 4** (Zangwill's Convergence Theorem). *Let  $A : X \rightarrow 2^X$  be a point-to-set algorithm acting on  $X$ . Given  $x_0 \in X$ , generate a sequence  $\{x_k\}_{k=1}^\infty$  such that  $x_{k+1} \in A(x_k)$  for every  $k$ . Let  $\Gamma \subset X$  be a solution set, and suppose that the following hold.*

- (i) *The sequence  $\{x_k\} \subset S \subset X$  for a compact set  $S$ .*
- (ii) *There exists a continuous function  $Z$  on  $X$  such that if  $x \notin \Gamma$  then  $Z(y) < Z(x)$  for all  $y \in A(x)$ , and if  $x \in \Gamma$  then  $Z(y) \leq Z(x)$  for all  $y \in A(x)$ . The function  $Z$  is called a descent function.*
- (iii) *The algorithm  $A$  is closed on  $X \setminus \Gamma$ .*

Then every convergent subsequence of  $\{x_k\}$  tends to a point in the solution set  $\Gamma$ .

Our algorithm is the update function  $T$ . We define our solution set as

$$\Gamma = \left\{ (R, \mathbb{M}) : J(R, \mathbb{M}) < J(\hat{R}, \hat{\mathbb{M}}) \forall (\hat{R}, \hat{\mathbb{M}}) \in B((R, \mathbb{M}), r) \right\}$$

for some  $r > 0$ , where the ball surrounding  $R$  is the Euclidean ball in  $\mathbb{R}^{nc}$  and the ball surrounding  $\mathbb{M}$  is  $\cup_{k=1}^c B_{W_2}(\mathbb{M}_k, r)$ . This set contains the local minima and saddle points of the cost function [3]. We wish to show that our cost function  $J(R, \mathbb{M})$  is the descent function  $Z$ . We proceed by verifying each of the requirements for Zangwill's Convergence Theorem.

**Lemma 5.** *Every iterate  $T^{(l)}(R, \mathbb{M}) \in [0, 1]^{nc} \times \text{conv}(\mathbb{D})^c$ , where*

$$\text{conv}(\mathbb{D}) = \bigcup_{k=1}^c \bigcup_{\gamma_j} \bigcup_{i=1}^m \text{conv}\{\gamma_j(y^{(i)}) : j = 1, \dots, n\},$$

with  $\gamma_j$  a bijection  $\mathbb{M}_k \rightarrow \mathbb{D}_j$  and  $\text{conv}\{\gamma_j(y^{(i)}) : j = 1, \dots, n\}$  the ordinary convex hull in the plane. Furthermore,  $[0, 1]^{nc} \times \text{conv}(\mathbb{D})^c$  is compact.

*Proof.* By construction, every  $r_{jk} \in [0, 1]$ . Since  $j = 1, \dots, n$  and  $k = 1, \dots, c$ , we can view  $R$  as a point in  $[0, 1]^{nc}$ , and so every iterate of  $R$  is in  $[0, 1]^{nc}$ . We shall show that for a fixed  $k$  and a fixed bijection  $\gamma_j : \mathbb{M}_k \rightarrow \mathbb{D}_j$ , each updated  $y^{(i)}$  is contained in a convex combination of  $\{\gamma_j(y^{(i)}) : j = 1, \dots, n\}$ . Where  $\gamma_j(y^{(i)}) = \Delta$ , let  $\gamma_j(y^{(i)}) = w_\Delta$  as defined in (4), as this is the update point we use for the diagonal. Since there are a finite number of off-diagonal points, each updated  $\mathbb{M}_k$  is therefore contained in the union over all bijections and all points  $y^{(i)}$  of the convex combination of  $\{\gamma_j(y^{(i)}) : j = 1, \dots, n\}$ . By also taking the union over each  $k$ , we show that every iterate of  $\mathbb{M}$  must be contained in the finite triple-union of the convex combination of each possible bijection. To show that each updated  $y^{(i)}$  is contained in a convex combination of  $\{\gamma_j(y^{(i)}) : j = 1, \dots, n\}$ , recall that  $y^{(i)} = \left( \sum_{j=1}^n r_{jk}^2 \right)^{-1} \sum_{j=1}^n r_{jk}^2 \gamma_j(y^{(i)})$ . Letting  $t_j^{(i)} = r_{jk}^2 \left( \sum_{j=1}^n r_{jk}^2 \right)^{-1}$ , clearly each  $t_j^{(i)} > 0$  and  $\sum_{j=1}^n t_j^{(i)} = 1$ . Therefore  $T^{(l)}(R, \mathbb{M}) \in [0, 1]^{nc} \times \text{conv}(\mathbb{D})^c$  for each  $l = 0, 1, \dots$ .

Now,  $[0, 1]$  is closed and bounded, so is compact. The convex hull of points in the plane is closed and bounded, so  $\text{conv}\{\gamma_j(y^{(i)}) : j = 1, \dots, n\}$  is compact. Since finite unions and finite direct products of compact sets are compact,  $[0, 1]^{nc} \times \text{conv}(\mathbb{D})^c$  is also compact.  $\square$

**Lemma 6.** *The cost function  $J(R, \mathbb{M})$  is a descent function, as defined in Theorem 4(ii).*

*Proof.* The cost function  $J$  is continuous, as it a sum, product and composition of continuous functions. Furthermore, we have that for any  $(R, \mathbb{M}) \notin \Gamma$ ,

$$J(T(R, \mathbb{M})) = J(F \circ G(R), G(R)) < J(R, G(R)) < J(R, M),$$

where the first inequality is due to Proposition 1 in [2], and the second inequality comes from the definition of the Fréchet mean. If  $(R, \mathbb{M}) \in \Gamma$  then the strict inequalities include equality throughout.  $\square$

**Theorem 7.** *For any  $(R, \mathbb{M})$ , every convergent subsequence of  $\{T^{(l)}(R, \mathbb{M}) : l = 0, 1, \dots\}$  tends to a local minimum or saddle point of the cost function  $J$ .*

*Proof.* We proceed with Zangwill's Convergence Theorem. Our algorithm is the update function  $T$ , our solution set is the set of all local minima, and our descent function is the cost function  $J(R, \mathbb{M})$ . By Lemma 5, every iterate in contained within a compact set. By Lemma 6,  $J$  is a descent function. Finally, since our function  $T$  only maps points in the plane to points in the plane, it is a closed map. The theorem follows by applying Theorem 4.  $\square$

## B Convergence of the Fréchet mean algorithm

Recall that the Fréchet mean is computed by finding the arg min of

$$F(\hat{\mathbb{D}}) = \sum_{j=1}^n r_{j,k}^2 F_j(\hat{\mathbb{D}}), \text{ with } F_j(\hat{\mathbb{D}}) = W_2(\hat{\mathbb{D}}, \mathbb{D}_j)^2, \quad (5)$$

for fixed  $k$ . We start by recounting work in [29], which this section adapts for the weighted Fréchet mean.<sup>5</sup> The proofs we're adapting use a gradient descent technique to prove local convergence. In order to use their techniques, we need to define a differential structure on the space of persistence diagrams.

By Theorem 2.5 in [29], the space of persistence diagrams  $\mathcal{D}_{L^2} = \{\mathbb{D} : W_2(\mathbb{D}, \Delta) < \infty\}$  is a non-negatively curved Alexandrov space. An optimal bijection  $\gamma : \mathbb{D}_1 \rightarrow \mathbb{D}_2$  induces a unit-speed geodesic  $\phi(t) = \{(1-t)x + t\gamma(x) : x \in \mathbb{D}_1, 0 \leq t \leq 1\}$ . For a point  $\mathbb{D} \in \mathcal{D}_{L^2}$  we define the tangent cone  $T_{\mathbb{D}}$ . Define  $\hat{\Sigma}_{\mathbb{D}}$  as the set of all non-trivial unit-speed geodesics emanating from  $\mathbb{D}$ . Let  $\phi, \eta \in \hat{\Sigma}_{\mathbb{D}}$  and define the angle between them as

$$\angle_{\mathbb{D}}(\phi, \eta) = \arccos \left( \lim_{s,t \downarrow 0} \frac{s^2 + t^2 - W_2(\phi(s), \eta(t))^2}{2st} \right) \in [0, \pi]$$

when the limit exists. Then the space of directions  $(\Sigma_{\mathbb{D}}, \angle_{\mathbb{D}})$  is the completion of  $\hat{\Sigma}_{\mathbb{D}} / \sim$  with respect to  $\angle_{\mathbb{D}}$ , with  $\phi \sim \eta \iff \angle_{\mathbb{D}}(\phi, \eta) = 0$ . We now define the tangent cone as

$$T_{\mathbb{D}} = (\Sigma_{\mathbb{D}} \times [0, \infty)) / (\Sigma_{\mathbb{D}} \times \{0\}).$$

Given  $u = (\phi, s), v = (\eta, t)$ , we define an inner product on the tangent cone by

$$\langle u, v \rangle = st \cos \angle_{\mathbb{D}}(\phi, \eta).$$

Now, for  $\alpha > 0$  denote the space  $(\mathcal{D}_{L^2}, \alpha W_2)$  as  $\alpha \mathcal{D}_{L^2}$  and define the map  $i_{\alpha} : \alpha \mathcal{D}_{L^2} \rightarrow \mathcal{D}_{L^2}$ . For an open set  $\Omega \subset \mathcal{D}_{L^2}$  and a function  $f : \Omega \rightarrow \mathbb{R}$ , the differential of  $f$  at  $\mathbb{D} \in \Omega$  is defined by  $d_{\mathbb{D}}f = \lim_{\alpha \rightarrow \infty} \alpha(f \circ i_{\mathbb{D}} - f(\mathbb{D}))$ . Finally, we say that  $s \in T_{\mathbb{D}}$  is a supporting vector of  $f$  at  $\mathbb{D}$  if  $d_{\mathbb{D}}f(x) \leq -\langle s, x \rangle$  for all  $x \in T_{\mathbb{D}}$ .

**Lemma 8.** *The following two results are proven in [29].*

<sup>5</sup>In [29], the Fréchet mean is defined as the arg min of the Fréchet function  $F(\hat{\mathbb{D}}) = \int W_2(\hat{\mathbb{D}}, \mathbb{D}_j)^2 d\rho(\hat{\mathbb{D}})$  with the empirical measure  $\rho = n^{-1} \sum_{j=1}^n \delta_{\mathbb{D}_j}$ . We are using the empirical measure  $\rho = \left( \sum_{j=1}^n r_{jk}^2 \right)^{-1} \sum_{j=1}^n r_{jk}^2 \delta_{\mathbb{D}_j}$ , but for ease we drop the scalar  $\left( \sum_{j=1}^n r_{jk}^2 \right)^{-1}$  as it is positive, so doesn't affect the minimum of the function.

(i) Let  $\mathbb{D} \in \mathcal{D}_{L^2}$ . Let  $F_j(\hat{\mathbb{D}}) = W_2(\hat{\mathbb{D}}, \mathbb{D}_j)^2$ . Then if  $\phi$  is a distance-achieving geodesic from  $\mathbb{D}$  to  $\hat{\mathbb{D}}$ , then the tangent vector to  $\phi$  at  $\mathbb{D}$  of length  $2W_2(\hat{\mathbb{D}}, \mathbb{D})$  is a supporting vector at  $\mathbb{D}$  of  $f$ .

(ii) If  $\mathbb{D}$  is a local minimum of  $f$  and  $s$  is a supporting vector of  $f$  at  $\mathbb{D}$ , then  $s = 0$ .

If there is a unique optimal matching  $\gamma_{\mathbb{D}_1}^{\mathbb{D}_3} : \mathbb{D}_1 \rightarrow \mathbb{D}_3$ , we say that it is induced by an optimal matching  $\gamma_{\mathbb{D}_1}^{\mathbb{D}_2} : \mathbb{D}_1 \rightarrow \mathbb{D}_2$  if there exists a unique optimal matching  $\gamma_{\mathbb{D}_2}^{\mathbb{D}_3} : \mathbb{D}_2 \rightarrow \mathbb{D}_3$  such that  $\gamma_{\mathbb{D}_1}^{\mathbb{D}_3} = \gamma_{\mathbb{D}_2}^{\mathbb{D}_3} \circ \gamma_{\mathbb{D}_1}^{\mathbb{D}_2}$ . Proposition 3.2 from [29] states that an optimal matching at a point is also locally optimal. In particular, it states the following.

**Lemma 9.** Let  $\mathbb{D}_1, \mathbb{D}_2 \in \mathcal{D}_{L^2}$  such that there is a unique optimal matching from  $\mathbb{D}_1$  to  $\mathbb{D}_2$ . Then there exists an  $r > 0$  such that for every  $\mathbb{D}_3 \in B_{W_2}(\mathbb{D}_2, r)$ , there is a unique optimal pairing from  $\mathbb{D}_2$  to  $\mathbb{D}_3$  that is induced by the matching from  $\mathbb{D}_1$  to  $\mathbb{D}_2$ .

The following theorem proves that our algorithm converges to a local minimum of the Fréchet function.

**Theorem 10.** Given diagrams  $\mathbb{D}_j$ , membership values  $r_{jk}$ , and the Fréchet function  $F$  defined in (5), then  $\mathbb{M}_k = \{y^{(i)}\}_{i=1}^m$  is a local minimum of  $F$  if and only if there is a unique optimal pairing from  $\mathbb{M}_k$  to each of the  $\mathbb{D}_j$ , denoted  $\gamma_j$ , and each  $y^{(i)}$  is updated via (4).

*Proof.* First assume that  $\gamma_j$  are optimal pairings from  $\mathbb{M}_k$  to each  $\mathbb{D}_j$ , and let  $s_j$  be the vectors in  $T_{\mathbb{M}_k}$  that are tangent to the geodesics induced by  $\gamma_j$  and are distance-achieving. Then by Lemma 8(i), each  $2s_j$  is a supporting vector for the function  $F_j$ . Furthermore,  $2 \sum_{j=1}^n r_{jk}^2 s_j$  is a supporting vector for  $F$ , as for any  $\hat{\mathbb{D}}$ ,

$$\begin{aligned} d_{\mathbb{M}_k} F(\hat{\mathbb{D}}) &= d_{\mathbb{M}_k} \left( \sum_{j=1}^n r_{jk}^2 F_j(\hat{\mathbb{D}}) \right) = \sum_{j=1}^n r_{jk}^2 d_{\mathbb{M}_k} F_j(\hat{\mathbb{D}}) \\ &\leq \sum_{j=1}^n -r_{jk}^2 \langle 2s_j, \hat{\mathbb{D}} \rangle = - \left\langle 2 \sum_{j=1}^n r_{jk}^2 s_j, \hat{\mathbb{D}} \right\rangle. \end{aligned}$$

By Lemma 8(ii),  $2 \sum_{j=1}^n r_{jk}^2 s_j = 0$ . Putting  $s_j = \gamma_j(y^{(i)}) - y^{(i)}$  and rearranging gives that  $y^{(i)}$  updates via (4), as required. Note that when  $\gamma_j(y^{(i)}) = \Delta$ , we let  $\gamma_j(y^{(i)}) = w_\Delta$  as defined in (4), because this minimises the transportation cost to the diagonal. Now suppose that  $\gamma_j$  and  $\tilde{\gamma}_j$  are both optimal pairings. Then by the above argument  $\sum_{j=1}^n r_{jk}^2 s_j = \sum_{j=1}^n r_{jk}^2 \tilde{s}_j = 0$ , implying that  $s_j = \tilde{s}_j$  and so  $\gamma_j = \tilde{\gamma}_j$ . Therefore the optimal pairing is unique.

To prove the opposite direction, assume that  $\mathbb{M}_k = \{y^{(i)}\}$  locally minimises the Fréchet function  $F$ . Observe that for a fixed bijection  $\gamma_j$ , we have that

$$\begin{aligned} F(\mathbb{M}_k) &= \sum_{j=1}^n r_{jk}^2 W_2(\mathbb{M}_k, \mathbb{D}_j)^2 \\ &= \sum_{j=1}^n r_{jk}^2 \left( \inf_{\gamma_j: \mathbb{M} \rightarrow \mathbb{D}_j} \sum_{y \in \mathbb{M}_k} \|y - \gamma_j(y)\|^2 \right) \\ &= \sum_{j=1}^n r_{jk}^2 \sum_{i=1}^m \|y^{(i)} - x_j^{(i)}\|^2 \\ &= \sum_{i=1}^m \left( \sum_{j=1}^n r_{jk}^2 \|y^{(i)} - x_j^{(i)}\|^2 \right). \end{aligned}$$

The final term in brackets is non-negative, and minimised exactly when  $y^{(i)}$  is updated via (4). Furthermore, the unique optimal pairing from  $\mathbb{M}_k$  to each of the  $\mathbb{D}_j$ 's is the same for every  $\hat{\mathbb{M}}$  within

the ball  $B_{W_2}(\mathbb{M}_k, r)$  for some  $r > 0$ , by Lemma 9. Therefore, if  $\mathbb{M}_k$  is a local minimum of  $F$ , then the  $y^{(i)}$ 's are equal to the values found by taking the optimal pairings  $\gamma_j$  and calculating the weighted means of  $\gamma_j(y^{(i)})$  with the weights  $r_{jk}^2$ , as required. It will remain a minimum as long as the matching stays the same, which happens in the ball  $B_{W_2}(\mathbb{M}_k, r)$ , so we are done.  $\square$

## C Experimental details

### C.1 Synthetic data

The membership values for the synthetic datasets are in Table 3. Datasets 1-3 are the datasets of noise, datasets 4-6 are the datasets with one ring, and datasets 7-9 are the datasets with two rings. We ran our algorithm for 20 iterations.

Table 3: Membership values for the synthetic dataset

Dataset	1	2	3	4	5	6	7	8	9
Cluster 1	0.6336	0.5730	0.5205	0.2760	0.2503	0.1974	0.2921	0.2128	0.2292
Cluster 2	0.1768	0.2057	0.2327	0.5361	0.5329	0.6371	0.2452	0.2291	0.1822
Cluster 3	0.1900	0.2212	0.2468	0.1879	0.2169	0.1655	0.4627	0.5580	0.5885

For the timing experiments we divide the total number of points equally between four distributions, two of which are noise and two of which are shaped in a ring. Each clustering algorithm was run for five iterations on one core of a 2019 MacBook Pro with a 1.4GHz Intel Core i5. We included the time taken to compute the persistence diagrams in the running times.

### C.2 Lattice structures

The results obtained are in Tables 4-7. The fuzzy values for FPDCluster are given as floats, although in each case they converged to an absolute cluster. The Wasserstein barycentre clustering algorithms each have discrete labels. The correct labellings are for 1-3 and 4-6 to be clustered together in each case. We clustered the 2-PH diagrams. We denote a label as having been assigned by 1, or not assigned by 0. We ran each algorithm for five iterations. We obtained our datasets as cif files, converted them to xyz then csv files, to have a list of the coordinates of each atom in  $\mathbb{R}^3$ . We create three copies of each structure. For rotation, we rotate two of them by  $180^\circ$  around different axes. For reflection, we reflect two of them in different axes. For translation, we translate them up or down by the length of the unit-cell. We use our own python implementation of our FCM persistence diagram clustering algorithm, available at <https://github.com/tomogwen/fpdcluster>. For each of the other algorithms, we use the implementation provided at [https://github.com/bobye/WBC\\_Matlab](https://github.com/bobye/WBC_Matlab).

Table 4: Membership values for non-transformed datasets

		Cubic Structure Datasets						Carbon Allotrope Datasets					
		1	2	3	4	5	6	1	2	3	4	5	6
FPDCluster	Cluster 1	1.000	1.000	1.000	0.000	0.000	0.000	1.000	1.000	1.000	0.000	0.000	0.000
	Cluster 2	0.000	0.000	0.000	1.000	1.000	1.000	0.000	0.000	0.000	1.000	1.000	1.000
ADMM	Cluster 1	1	1	1	0	0	0	1	1	1	0	0	0
	Cluster 2	0	0	0	1	1	1	0	0	0	1	1	1
BADMM	Cluster 1	1	1	1	0	0	0	1	1	1	0	0	0
	Cluster 2	0	0	0	1	1	1	0	0	0	1	1	1
SubGD	Cluster 1	1	1	1	0	0	0	1	1	1	0	0	0
	Cluster 2	0	0	0	1	1	1	0	0	0	1	1	1
IterBP	Cluster 1	1	1	1	0	0	0	1	1	1	0	0	0
	Cluster 2	0	0	0	1	1	1	0	0	0	1	1	1
LP	Cluster 1	1	1	1	0	0	0	1	1	1	0	0	0
	Cluster 2	0	0	0	1	1	1	0	0	0	1	1	1

Table 5: Membership values for rotated datasets

		Cubic Structure Datasets						Carbon Allotrope Datasets					
		1	2	3	4	5	6	1	2	3	4	5	6
FPDCluster	Cluster 1	1.000	1.000	1.000	0.000	0.000	0.000	1.000	1.000	1.000	0.000	0.000	0.000
	Cluster 2	0.000	0.000	0.000	1.000	1.000	1.000	0.000	0.000	0.000	1.000	1.000	1.000
ADMM	Cluster 1	0	0	1	0	0	1	1	0	1	1	0	1
	Cluster 2	1	1	0	1	1	0	0	1	0	0	1	0
BADMM	Cluster 1	0	1	1	0	1	1	1	1	0	1	1	0
	Cluster 2	1	0	0	1	0	0	0	0	1	0	0	1
SubGD	Cluster 1	0	1	1	0	1	1	1	0	0	1	0	0
	Cluster 2	1	0	0	1	0	0	0	1	1	0	1	1
IterBP	Cluster 1	0	1	0	0	1	0	0	1	1	0	1	1
	Cluster 2	1	0	1	1	0	1	1	0	0	1	0	0
LP	Cluster 1	1	0	1	1	0	1	0	1	0	0	1	0
	Cluster 2	0	1	0	0	1	0	1	0	1	1	0	1

Table 6: Membership values for reflected datasets

		Cubic Structure Datasets						Carbon Allotrope Datasets					
		1	2	3	4	5	6	1	2	3	4	5	6
FPDCluster	Cluster 1	1.000	1.000	1.000	0.000	0.000	0.000	1.000	1.000	1.000	0.000	0.000	0.000
	Cluster 2	0.000	0.000	0.000	1.000	1.000	1.000	0.000	0.000	0.000	1.000	1.000	1.000
ADMM	Cluster 1	1	1	1	0	0	0	0	0	0	1	1	0
	Cluster 2	0	0	0	1	1	1	1	1	1	0	0	1
BADMM	Cluster 1	1	1	1	0	0	0	0	0	0	1	1	0
	Cluster 2	0	0	0	1	1	1	1	1	1	0	0	1
SubGD	Cluster 1	1	1	1	0	0	0	1	1	1	1	1	0
	Cluster 2	0	0	0	1	1	1	0	0	0	0	0	1
IterBP	Cluster 1	1	1	1	0	0	0	0	0	0	0	0	1
	Cluster 2	0	0	0	1	1	1	1	1	1	1	1	0
LP	Cluster 1	1	1	1	0	0	0	0	0	0	0	1	1
	Cluster 2	0	0	0	1	1	1	1	1	1	1	0	0



Table 7: Membership values for translated datasets

		Cubic Structure Datasets						Carbon Allotrope Datasets					
		1	2	3	4	5	6	1	2	3	4	5	6
FPDCluster	Cluster 1	1.000	1.000	1.000	0.000	0.000	0.000	1.000	1.000	1.000	0.000	0.000	0.000
	Cluster 2	0.000	0.000	0.000	1.000	1.000	1.000	0.000	0.000	0.000	1.000	1.000	1.000
ADMM	Cluster 1	0	0	1	0	0	1	0	0	1	0	0	1
	Cluster 2	1	1	0	1	1	0	1	1	0	1	1	0
BADMM	Cluster 1	0	1	0	1	1	0	1	1	0	1	1	0
	Cluster 2	1	0	1	0	0	1	0	0	1	0	0	1
SubGD	Cluster 1	0	0	1	0	0	1	0	1	0	0	1	0
	Cluster 2	1	1	0	1	1	0	1	0	1	1	0	1
IterBP	Cluster 1	0	1	0	0	1	0	0	0	1	0	0	1
	Cluster 2	1	0	1	1	0	1	1	1	0	1	1	0
LP	Cluster 1	0	0	1	0	0	1	1	0	1	1	0	1
	Cluster 2	1	1	0	1	1	0	0	1	0	0	1	0